Author Manuscript

Author Manuscript

Author Manuscript

Author Manuscript

HHS Public Access

Author manuscript

Environ Sci Technol. Author manuscript; available in PMC 2017 July 05.

Published in final edited form as:

Environ Sci Technol. 2016 July 05; 50(13): 7208–7217. doi:10.1021/acs.est.6b01881.

Chemical dissolution pathways of MoS_2 nanosheets in biological and environmental media

Zhongying Wang[1], **Annette von dem Bussche**[2], **Yang Qiu**[1], **Thomas M. Valentin**[1], **Kyle Gion**[1], **Agnes B. Kane**[2,3], and **Robert H. Hurt**[1,3,*]

[1]School of Engineering, Brown University, Providence, Rhode Island 02912

[2]Department of Pathology and Laboratory Medicine, Brown University, Providence, Rhode Island 02912

[3]Institute for Molecular and Nanoscale Innovation, Brown University, Providence, Rhode Island 02912

Abstract

Material stability and dissolution in aqueous media are key issues to address in the development of a new nanomaterial intended for technological application. Dissolution phenomena affect biological and environmental persistence; fate, transport, and biokinetics; device and product stability; and toxicity pathways and mechanisms. This article shows that MoS_2 nanosheets are thermodynamically and kinetically unstable to O_2-oxidation under ambient conditions in a vareity of aqueous media. The oxidation is accompanied by nanosheet degradation and release of soluble molybdenum and sulfur species, and generates protons that can colloidally destabilize the remaining sheets. The oxidation kinetics are pH-dependent, and a kinetic law is developed for use in biokinetic and environmental fate modelling. MoS_2 nanosheets fabricated by chemical exfoliation with n-butyl-lithium are a mixture of 1T (primary) and 2H (secondary) phases and oxidize rapidly with a typical half-life of 1–30 days. Ultrasonically exfoliated sheets are in pure 2H phase, and oxidize much more slowly. Cytotoxicity experiments on MoS_2 nanosheets and molybdate ion controls reveal the relative roles of the nanosheet and soluble fractions in the biological response. These results indicate that MoS_2 nanosheets will not show long-term persistence in living systems and oxic natural waters, with important implications for biomedical applications and environmental risk.

Graphical Abstract

Corresponding Author: Robert H. Hurt, Robert_Hurt@brown.edu, Tel: 401-863-2685.

Supporting Information

Additional information and figures. This material is available free of charge via the Internet at http://pubs.acs.org.

Author Manuscript Author Manuscript Author Manuscript Author Manuscript

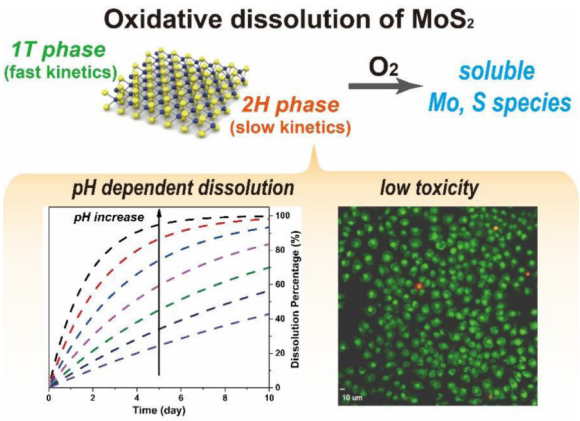

Keywords

transition metal dichalcogenides; oxidation; dissolution; nanotoxicology

Introduction

Environmental stability is one of the most important properties of a newly discovered nanomaterial targeted at large-scale application. Degradation affects the lifetime and reliability of the material and its derived products or devices, and can constrain operating windows and limit application fields. Stability in aqueous phases is of special importance for assessing environmental and health effects, which is a key step in the development pathway, as a new chemical substance moves from the laboratory to large-scale manufacturing and use. Chemical degradation pathways in aqueous phases determine if a new nanomaterial will be persistent upon release into the natural environment with the potential for long-term impacts, or will degrade into molecular species that no longer pose a material-specific or "nano-specific" risk.

In the human body, nanomaterial stability in biological fluid phases affects biopersistence, biokinetics, lung and renal clearance, and the proper design and interpretation of experiments to characterize toxicity. Inorganic materials that degrade typically produce a pool of soluble species that co-exist with the solid in biological media, and can initiate toxicity pathways independently of, or in parallel with, the solid phase.[1–9] As free molecular species, these soluble products often act with high bioavailability and molecular specificity at target receptors. Indeed, many nanomaterials are now known to exert their biological effects wholly, or in part, through the action of co-existing ions, with outstanding examples being nanoscale Ag,[1, 9–11] ZnO,[2, 12, 13] Cu,[5, 14] and Ni.[6] If left uncharacterized or uncontrolled during sample storage and preparation, these ion pools can lead to varying and confounding toxicity data, or the incorrect interpretations of molecular toxicity mechanisms.[4, 15] In contrast, materials that are stable are often not effectively cleared from the lung or from the bloodstream and show long-term bio-persistence that is of concern for the induction of diseases after a long latent period, such as mesothelioma or lung cancer associated with asbestos fiber exposure. Overall, identifying aqueous-phase degradation

Author Manuscript Author Manuscript Author Manuscript Author Manuscript

pathways, kinetics, and products, should be one of the first goals in characterizing a new nanomaterial targeted for large-scale technological application.

Among the most promising next-generation nanomaterials are the 2D transition metal dichalcogenides (TMDs), which are fabricated in monolayer or few-layer form by colloidal growth, vapor-phase growth, or exfoliation of bulk layered parent crystals.[7, 16–23] Molybdenum disulfide (MoS_2), for example, consists of covalently bonded atomic trilayers of sulfur-molybdenum-sulfur, which in the bulk crystal are stacked with van der Waals gaps that allow exfoliation by a variety of chemical or ultrasonic methods.[18, 19, 24, 25] MoS_2 has received tremendous attention because its monolayer form exhibits a direct band gap, while the bulk form exhibits only an indirect band gap.[26] Exfoliation thus induces an indirect-to-direct conversion with a remarkable enhancement of light absorption efficiency and promising applications in electronics and optoelectronics.[19, 27–30]

We became interested in the stability and degradation of TMD materials as a logical early step in the understanding of their biological and environmental behaviors. Traditionally TMDs are regarded as quite stable materials because of the lack of dangling bonds in the electron-filled shells of terminating chalcogen atoms.[31] MoS_2 is listed as “water insoluble” in standard chemical reference works,[32] and has been reported in many studies to be stable to oxidation under ambient conditions.[33–35] Recent modelling results suggest that the ambient stability of MoS_2 is due to kinetic limitations associated with the initial dissociative adsorption of O_2 on MoS_2 surfaces.[34]

Under more extreme conditions, far from ambient, oxidation of TMD nanosheets has been well documented.[36, 37] Yamamoto *et al.* reported the formation of molybdenum oxide (MoO_3) on an atomically thin MoS_2 surface after exposure to oxygen at temperatures above 340 °C, and demonstrated that the oxidation starts at MoS_2 defects sites.[36] At a comparable temperature, WSe_2 nanosheets were observed to form WO_3 initiating from the nanosheet edge and propagating inward. The reaction rate decreased with decreasing temperature and became negligible below 200 °C.[37] While it is clear that MoS_2 does not oxidize readily in ambient air, a recent study focused on long-term effects documented degradation over time scales of six months to one year, and discussed its important implications for electronic applications.[38] Also relevant is an older report on formation of a passivating oxide layer on the surface of bulk MoS_2, which prevents stoichiometric (full) conversion to the oxide in the dry state.[35] There are also chalcogen-based 0D nanoparticles such as CdSe quantum dots (QDs), and studies have shown quenching and chemical degradation during their use under physiologic conditions, which was ascribed to chemical oxidation of sulfur or selenium atoms on the QD surface.[39, 40]

Despite the importance of MoS_2, we were not able to find any studies relating to the long-term stability or persistence of MoS_2 in aqueous phases relevant to biological systems or the natural environment. A recent review article presented a thermodynamic analysis suggesting that MoS_2 and other TMD nanosheet materials would be unstable to oxidative dissolution in O_2-containing aqueous media, but no data were available to reveal if the kinetics are sufficiently fast for measureable degradation over relevant time scales.[7] If strong oxidizing agents such as hydroxyl radicals or H_2O_2 are introduced, then etching of MoS_2 is indeed

Author Manuscript Author Manuscript Author Manuscript Author Manuscript

observed and leads to formation of MoS_2 quantum dots and soluble molybdenum species,[41] but of course these data are not directly relevant to the reaction with O_2 as the sole oxidant.

We therefore undertook a systematic study of the long-term stability and oxidative dissolution of MoS_2 nanosheets in biologically and environmentally relevant aqueous media with and without dissolved molecular oxygen. It will be shown that MoS_2 nanosheets undergo a clear O_2-driven oxidative dissolution process with kinetics that depend on pH, exfoliation method, phase, and processing history with important implications for environmental health and safety.

Materials and Methods

Preparation of 2D MoS_2 nanosheets

A dispersion of MoS_2 nanosheets was prepared by organolithium intercalation followed by forced hydration19 and referred to here as "chemically exfoliated MoS_2" (ce-MoS_2). Ultrasonically exfoliated nanosheets (ue-MoS_2) were produced with a surfactant-assisted exfoliation similar as that developed by Smith *et al.*[18] Excess surfactant (sodium cholate) was removed by ultrafiltration using Amicon centrifugal ultrafilter (Ultra-15, 3K). The conversion of 1T component in ce-MoS_2 to 2H phase was carried out in hydrothermal reaction.[42] Specially, 10 mL of ce-MoS_2 (50 ppm of Mo) was added to a 20 mL Teflon-lined autoclave and heated at 200 °C for 4 h. A low concentration of ce-MoS_2 nanosheet precursor was used to minimize aggregation and its potential effects on the oxidation rate of the converted MoS_2 nanosheets. Additional synthesis and characterization details can be found in Supporting Information.

Dissolution of 2D MoS_2 nanosheets in aqueous solutions

To investigate the long-term stability of ce-MoS_2, dispersion samples at high (~ 210 ppm of Mo), medium (~ 42 ppm of Mo) and low concentration (~ 8.5 ppm of Mo) were prepared and placed under ambient conditions (air exposure, room temperature) for fixed times. To investigate the effect of oxygen, control groups were prepared and the timed incubation was carried out in a nitrogen-filled glovebox. After a pre-determined incubation time, the solids were separated from the dissolved species using centrifugal ultrafiltration[43] and the total soluble Mo concentrations determined by ICP-AES (JY 2000 Ultrace). During the dissolution reactions, the dispersion pH was monitored with a pH electrode (Orion 8165BNWP, Thermo Scientific). To investigate the effects of pH on the oxidative dissolution of MoS_2 nanosheets, MoS_2 nanosheet dispersions (~ 8.5 ppm of Mo) were incubated in various buffer solutions: 50 mM acetate buffers (at pH 3.5 and 5.7), 50 mM HEPES buffer (pH 8) and 50 mM phosphate buffer (pH 10.9) To study media effects, MoS_2 dispersions were added to a natural fresh water simulant (50 mM humic acid in acetate buffer, pH 5.7), RPMI 1640 cell culture medium (Sigma 51536C, pH 7.4) and synthetic seawater (Sigma S9148, pH 8.2). After fixed period of time, the dissolved Mo species were isolated and measured by ICP-AES as previously described.

Author Manuscript Author Manuscript Author Manuscript Author Manuscript

Cell Toxicity Studies

Murine macrophages (ATCC: TIB-67) and human lung epithelial cells (ATCC: HTB-177) were plated into 96 well plates and incubated overnight, then exposed to different concentrations of sodium molybdate (1, 3, 5 or 8 mM) or ce-MoS_2 (up to 80 μg/mL) for 24, 48 or 72 hours. Cells were washed once, and then cell viability was assessed after 24, 48 and 72 hours using dehydrogenase activity assay Wst 8 (CCK-8; Dojindo; CK04-05). 10,000 lung epithelial cells or 25,000 macrophages were seeded and exposed, and the cells were washed once with cell culture medium and then exposed to 100 μl/well phenol red-free medium containing WST-8 substrate diluted to a concentration of 1:10 for one hour to lung epithelial cells or for 3 hours to murine macrophages. The absorbance was quantified at 450 nm using a Spectramax M2 (Molecular Devices).

Visualization of cell death in murine macrophages and human lung epithelial cells was conducted using ethidium-homodimer /Syto 10 stain after exposure to sodium molybdate (1, 3, 5 or 8 mM) or ce-MoS_2 (up to 80 μg/mL) for 24 hours. Cells were washed once and incubated with 5 μM/ml Syto10/ and 1 μg/ml ethidium homodimer (Invitrogen) in phosphate buffered saline for 5 min (macrophages) or 15 min (lung epithelial cells). Images were visualized using a spinning-disk Olympus confocal fluorescence (Model IX81) motorized inverted research microscope.

Results and Discussion

Preparation and characterization of MoS_2 nanosheets

While chemical exfoliation achieves monolayer MoS_2 in high yield, the Li intercalation is reported to induce phase changes and alteration of some pristine nanosheet properties.[19] Specifically, the organolithium reagent is reported to transfer electrons to MoS_2 during the intercalation process to produce negative charges on the nanosheets that can be directly observed in aqueous dispersions by measurement of electrophoretic mobility.[44, 45] Lithium intercalation has also been reported to induce structural distortion that converts a fraction of the Mo atoms from trigonal prismatic coordination (the thermodynamically stable and semiconducting 2H phase, Fig. 1d) to octahedral coordination (the metastable metallic 1T phase, Fig. 1b).[44, 46] Another widely used fabrication method for 2D MoS_2 involves ultrasonic exfoliation using probe sonication.[18] The ue-MoS_2 nanosheets lack the large negative surface charge but can be colloidally stabilized in aqueous media by the surfactant sodium cholate.[18] The ultrasonic method does not typically yield high concentrations of monolayers, but does preserve the naturally occurring 2H phase. Both types of MoS_2 nanosheet materials are of interest to the field[16, 19, 24, 47–54] and are thus relevant to environmental and health implications studies.[55–58] Atomic Force Microscopy (AFM) in Fig. 1a reveals as-prepared ce-MoS_2 nanosheets with lateral dimension ~ 250 nm, and average thickness ~ 1.2 nm in agreement with the reported values for monolayer MoS_2 (see additional AFM images and lateral size distributions in Fig. S1).[19, 45] As-prepared ue-MoS_2 products are few-layer nanosheets with average lateral size from 100 to 150 nm as shown in Fig. 1c and 2–5 S-Mo-S trilayers (see detailed characterization in Fig. S1).

Author Manuscript Author Manuscript Author Manuscript Author Manuscript

Due to the differences in electronic structures, ce-MoS_2 and ue-MoS_2 samples can be differentiated easily by UV-vis spectroscopy. Fig. 1e shows that few-layer ue-MoS_2 nanosheets display absorption bands at ~390, 440, 610 and 670 nm (blue trace), consistent with values reported for the 2H phase,[19, 42] while ce-MoS_2 spectra are nearly featureless. Further, semi-quantitative analysis of the phase composition was carried out using XPS, and the Mo 3d and S 2p regions are shown in Fig. 1f for both types of MoS_2 nanosheets. The Mo 3d spectrum of the ue-MoS_2 sample consists of peaks at ~ 229.3 and 232.4 eV, which correspond to Mo^{4+} $3d_{5/2}$ and $3d_{3/2}$ components of the 2H phase confirming that the ultrasonic exfoliation process does not alter the pristine 2H polymorph. In the ce-MoS_2 sample, however, the overall peaks are shifted to lower binding energies and deconvolution reveals the presence of 2H phase peaks and the emergence of additional peaks at lower binding energies, which arise from 1T phase.[19, 42] The difference of these two phases in binding energies has been reported to be ~ 0.7 to 0.9 eV.19, 42 Similarly, in the S 2p region, ue-MoS_2 shows only the 2H component with doublet peaks S $2p_{1/2}$ and $2p_{3/2}$, at ~163.2 and 162.1 eV, respectively. Meanwhile additional peaks are also found in the ce-MoS_2 sample at the positions ~ 0.8 eV lower with respect to 2H phase peaks. Quantification using the 1T and 2H polymorph spectral fits gives ~61% 1T phase and ~59% 2H phase in the as-prepared ce-MoS_2.

Oxidative dissolution and colloidal stability of ce-MoS_2 nanosheets

Wang *et al.*[7] showed recently that a range of TMD materials are thermodynamically unstable to oxidative dissolution in simple air-saturated aqueous phases at standard state and fixed pH. We first examine a wider range of conditions for MoS_2 and $MoSe_2$ using the approach of Chen and Wang,[59] and found that MoS_2 and $MoSe_2$ are both thermodynamically unstable to air oxidation over a wide range of pH and concentrations relevant to biological and environmental compartments (see Supporting Information, Table S1 and Figure S2 for details).

In the following, we use centrifugal ultrafiltration and ICP-AES analysis to directly track the time-resolved release of soluble species from ce-MoS_2 nanosheets and the time evolution of pH in both oxidizing and non-oxidizing aqueous environments. Figure 2a shows the concentration of soluble Mo species increasing steadily over time in air-saturated water, reaching ~50% of the total Mo in the sample after ~100 days. The dissolution process is suppressed in deoxygenated water (Fig. 2a, red trace), and the finite concentration of soluble Mo that is present at zero time likely reflects some pre-oxidation in the sample preparation and storage. In air-saturated water the pH decreases continuously indicating proton generation in the oxidation process, and the pH decrease is more pronounced at higher initial mass loadings of ce-MoS_2 (Fig. 2b). After 105-day incubation, the measured pH values of low and intermediate concentration samples (as shown in Fig. 2a and 2b) agree with anticipated values (3.5 and 2.9, respectively) from the total amount of Mo dissolved based on the reaction stoichiometry:

$$MoS_2+9/2O_2+3H_2O=MoO_4{}^{2-}+2SO_4{}^{2-}+6H^+ \quad (1)$$

Author Manuscript Author Manuscript Author Manuscript Author Manuscript

suggesting that molybdate ion (MoO_4^{2-}) is the main Mo-containing product. Analysis of other reaction products will be presented in a later section.

Additional experiments were carried out on bulk layered MoS_2 powders (~ 2 μm particle size) and the concentration of soluble Mo species was very low and approached the detection limit of ICP-AES even after 40-day incubation.(Supporting Information, Fig. S3) Other studies have shown that bulk MoS_2 powders are resistant to oxidation[31, 34] or form thin passivating oxide layers that prevent full stoichiometric oxidation under ambient conditions[35]. Bulk layered MoS_2 is described as a stable, insoluble material in a variety of standard references and property databases. Oxidative dissolution over these time scales appears to be a particular behavior of the nanosheet forms of MoS_2.

During the dissolution experiments we made the interesting observation that ce-MoS_2 nanosheets were colloidally stable in suspensions under all conditions except at the highest mass loading (210 ppm of Mo) after long-term exposure to oxygen in air-saturated water (Fig. 2c). There are relevant reports in the literature of colloidal stability loss in ce-MoS_2 nanosheets causing aggregation and restacking during storage.[45, 60] It is possible that oxidative or hydrolytic transformation of the MoS_2 solid phase is responsible for this loss of colloidal stability, but the patterns in our data suggest it is primarily due to electrostatic destabilization by reaction-generated protons. The colloidal stability of dispersed ce-MoS_2 has been attributed to the repulsive forces among negatively charged nanosheets, which arise from the electron transfer from organolithium reagents during intercalation.[61] Zeta potential measurements show −45 to −50 mV at neutral pH (Fig. 2d), similar to previous reports[45] and suggesting strong electrostatic stabilization initially.[62] Fig. 2d shows the pH-dependence of zeta potential, which reaches −28 mV at pH 1.6. This potential is near the typical threshold between electrostatic stabilization and aggregation, and indeed in this range we begin to observe aggregation. To further explore the stability threshold, dynamic light scattering was used to directly monitor the changes in effective nanosheet size (aggregate size) as pH is reduced by HCl addition (Fig. 2e). That transition in ce-MoS_2 dispersion occurs near pH 1.9 as indicated by the significant aggregate size growth in Fig. 2e at pH values below 1.9 but not above. Only the ce-MoS_2 dispersion with the highest nanosheet mass loading (210 ppm of Mo) and at the greatest extent of oxidation can generate sufficient protons to reach this pH, and only this sample shows the colloidal instability. Overall, these results show that ce-MoS_2 nanosheets in aqueous suspensions can undergo aggregation over time, and a sufficient explanation is electrostatic destabilization associated with proton release that is a by-product of the oxidative dissolution process.

Dissolution kinetics and complex media effects

The data from simple media experiments (Fig. 2) are not suitable for quantitative kinetic analysis due to changing pH. We hypothesized that the asymptotic behavior in Fig. 2 is the behavior of a self-limiting reaction that generates protons that inhibit further reaction. We therefore carried out ce-MoS_2 dissolution experiments in a range of buffer solutions: acetate buffer (pH 3.5 and 5.7), HEPES buffer (pH 8) and phosphate buffer (pH 10.9). The ionic strengths of the buffers were maintained sufficiently low to minimize nanosheet aggregation

Author Manuscript Author Manuscript Author Manuscript Author Manuscript

during dissolution measurements. The pH-dependent dissolution rates for ce-MoS_2 are shown in Fig. 3a, and give the following empirical kinetic equation:

$$-\frac{d[MoS_2]}{[MoS_2]*dt}=1.9\times[OH^-]^{0.17},1/d \quad (2)$$

where the rate is expressed in days^{-1} and OH^- is in mol/L units. The fitting is based on the dissolution data at low concentrations of monolayer ce-MoS_2, and may be used for the estimation of soluble species release in the low concentration regime most relevant to the environment and other biomedical applications.[49, 50] Fig. 3b shows the oxidative dissolution of ce-MoS_2 samples in selected simulants of environmental and biological media: natural fresh water (pH 5.7), cell culture medium/CCM (pH 7.4) and sea water (salinity: 3.2% by weight of salt, pH 8.2). These data are superimposed on the pH-dependent rates in simple media (dashed lines), and the comparisons show that the additional media components reduce dissolution rates. This may arise from the aggregation of ce-MoS_2 nanosheets in the high ionic strength buffers (sea water and CCM) and/or the presence of reducing agents (humic acid in natural fresh water and thiol functional groups in CCM). The effects are modest, however, and pH appears to be the most important factor influencing ce-MoS_2 oxidative dissolution rates.

Figure 3c shows that the ultrasonically exfoliated samples (ue-MoS_2) dissolve with much slower kinetics. A possible origin of the slower kinetics in ue-MoS_2 is the multilayer nature of this sample, which reflects the lower efficiency of the ultrasonic exfoliation route. We estimate the mean layer number, N_L, in ue-MoS_2 to be ~ 4 (see Fig. S1), but the difference in mass-specific total area, A, scales as $1/N_L$ and is not sufficient to explain the difference in Fig. 3c. It is also likely that the active sites for oxidative attack on MoS_2 reside on edges and basal defects,[36] and the edge sites may be expected to retain accessibility in multilayer stacks, so the active site concentration is likely to be even less sensitive to the stacking degree, N_L, and cannot fully explain the slow reaction rate for ue-MoS_2.

Since surface area cannot explain the kinetic differences between the chemically and ultrasonically exfoliated forms, we considered the effects of solid-state structure. Ue-MoS_2 sample consists solely of the stable 2H phase, while the ce-MoS_2 samples are mixed 2H / 1T phases and may also contain a higher concentration of defects formed by the violent chemical exfoliation.[45, 63] We conducted a series of experiments to explore the role of crystal structure of oxidation kinetics. First, annealing at moderate temperatures has been reported to convert the 1T phase back to the 2H phase.[19] Therefore, ce-MoS_2 nanosheets were converted to 2H-MoS_2 (ce-2H MoS_2) in a hydrothermal reaction[42] as evidenced by UV-vis characteristic peaks and XPS spectrum in Supporting Information, Fig. S5. The oxidative dissolution of this annealed sample is significantly inhibited relative to the original ce-MoS_2 under the same conditions (Fig. S5).

To further investigate the oxidation rate of each component polymorph (1T vs 2H), time-resolved studies were carried out to track the evolution of phase composition of the initially mixed ce-MoS_2 samples during oxidation. Selected ce-MoS_2 samples were incubated in

Author Manuscript Author Manuscript Author Manuscript Author Manuscript

relatively high pH buffer solution (~ 11.2) to minimize the reaction time needed. Fig. 4a shows, in time-resolved UV-vis spectra of ce-MoS_2 dispersion, the absorbance decreases in the entire range from 350 to 800 nm due to the oxidative dissolution of the sample. The characteristic peak of 2H at ~ 400 nm becomes more visible, however, even while the overall peak intensity decreases. Normalizing the spectra by the peak absorbance at ~ 350 (Fig. 4 b1) and ~800 nm (Fig. 4 b2) reveals that the 2H peak undergoes relative growth, which provides further evidence that the 1T component is selectively oxidized to enrich the 2H phase.

A semi-quantitative analysis is possible using time-resolved XPS spectra. The Mo 3d spectra in Fig. 4c reveal the convolution of 1T and 2H peaks shifted from as-prepared ce-MoS_2 to higher binding energies over time, and eventually, after 7-day dissolution, to the position that is typically considered to be pure 2H-MoS_2.[19] Similar trends can also be observed in the S 2p spectra. The convolution of the peaks from two phases shifts from 161.5 to 162.1 eV. A more apparent feature for the S 2p spectra is the evolution from broad peak contributed by both phases to distinguishable two peaks ascribed to 2H doublets. The XPS results demonstrate that the 1T component in ce-MoS_2 is preferentially degraded, leaving only the 2H phase after 7-day of oxidative dissolution. Continuous monitoring on the UV-vis spectra of ce-MoS_2 after 7-day exposure reveals further slow decrease, which indicates the 2H may also undergo oxidative dissolution but in a much slower manner, which is consistent with data in Fig. 3c. The ce-MoS_2 sample in Fig. 2a was also exposed to air for one full year, after which ICP analysis revealed ~90% of the total molybdenum as soluble species. Some nanosheets remained, however, and showed the characteristic peaks of the 2H phase (Fig. S6). This provides additional evidence for the preferential oxidation of the 1T phase, and the 1-yr persistence in this case reflects the low pH conditions in this experiment (~3) as well as the slow oxidation kinetics of the 2H component that forms the residual solid.

More work is needed to understand the molecular mechanism behind the variable oxidation reactivities observed for different types of MoS_2 nanosheets in this study. Higher reactivity correlates here with the presence of the 1T phase, and may be an intrinsic property of that phase associated with its characteristic Mo/S atomic arrangement and metallic nature. Alternatively, the higher reactivity of the ce-MoS_2 samples may reflect interaction with the organo-lithium reagent to create defects or negative charge that influence oxidation mechanism. The initiation of oxidative etching via intrinsic defects has been observed in mechanically exfoliated MoS_2 nanosheets annealed in oxygen.[36]

We were also interested in understanding the full reaction products of MoS_2 nanosheet oxidation. The biogeochemical literature contains some relevant information on bacterial mediated attack of bulk MoS_2 minerals. The general process of mineral bio-oxidation is referred to in this literature as “bioleaching” and can be either direct, or indirect involving a chemical mediator. Mineral oxidation usually occurs through multiple steps catalyzed by either bacterial enzymes or the chemical mediator.[64] For MoS_2, thiosulfate has been reported to form first, followed by further oxidation by ferric iron in a series of reactions generating soluble intermediate species (S_4O6^{2-}, $HSSSO_3^-$), and finally sulfate.[65] Faster oxidative bioleaching of MoS_2 was observed in samples of smaller particle size,[66] consistent with the expected role of surface area.

Author Manuscript Author Manuscript Author Manuscript Author Manuscript

To better define the reaction products in the present study, sulfur-based species appearing upon oxidative dissolution of ce-MoS_2 were measured by ICP-AES. Fig. 5a shows the percentage of dissolved sulfur species increasing over time until nearly complete dissolution is achieved at ~ 1 day. Again, a high pH buffer was used here to minimize reaction time and to increase the chances of observing any insoluble sulfur intermediates (*e.g.* sulfur(0), amorphous S) that over longer times may be further oxidized to sulfate. The soluble S/Mo molar ratio is observed to be < 2 in the early stages (possibly suggesting early formation of some insoluble S intermediate), but approaches 2 after 5 hours, indicating eventual conversion of the MoS_2 composition to all-soluble species.

Figure 5b shows contrasting behavior for $MoSe_2$ nanosheets prepared by organolithium intercalation and exfoliation. For $MoSe_2$ nanosheets, soluble Mo species (red trace) increase over time in a similar behavior to MoS_2, but the chalcogen, Se, does not appear in solution, suggesting the formation of insoluble Se(0). A similar behavior was reported by Zhang *et al.*, who studied the oxidation of Bi_2Se_3 nanosheets and observed red insoluble amorphous zero-valent selenium as a product that was stable to further oxidation.[67]

Cytotoxicity of MoS_2 nanosheets - implications of ion release

One immediate implication of the present results is the potential for ion release to mediate the biological response to MoS_2 nanosheets. Soluble ionic species that coexist with nanoparticles can be highly bioavailable and have been reported to be primary drivers of the cellular response to a number of nanomaterial systems, including ZnO, Ag, Cu and its oxides, Ni and NiO.[1, 3, 5, 6, 8–10, 12] The results of Figure 2–5 show that soluble Mo release occurs over time scales of days to weeks at biologically-relevant pH values, which places ce-MoS_2 nanosheets in the class of materials that exist as mixed suspensions of soluble ions and solids (nanosheets) during initial exposure, cellular uptake, and processing.

Here we studied the *in vitro* biological response of murine macrophages and human lung epithelial cells to ce-MoS_2 nanosheets. As described previously, both thermodynamics and the observed reaction stoichiometry suggest dissolution products contain molybdate, Mo(VI), so we chose a soluble molybdate salt (Na_2MoO_4) for the control experiment to understand ion effects. Figure 6b shows that the ce-MoS_2 nanosheet samples are not toxic to murine macrophages at doses up to 80 μg/ml. A similar behavior is observed in human lung epithelial cells (Fig. S7). A number of other studies have reported low toxicity for MoS_2 nanosheets,[56, 58] and they have been proposed for biomedical technologies including drug delivery, photothermal therapy, and imaging.[16, 49–51] Soluble molybdate controls show statistically significant cell viability loss at concentrations above 3 mM (Fig. 6a). This Mo concentration, however, is much higher than that achievable during nanosheet exposure, even if the sheets were to undergo complete dissolution (see orange bar that maps soluble Mo concentrations to fnanosheet dose). This comparison helps explain the low toxicity of MoS_2 nanosheets observed here and elsewhere - the nanosheets undergo oxidative dissolution, but the released molybdate ions have a low intrinsic toxicity at the material doses commonly used in nanotoxicology studies. Confocal fluorescence imaging demonstrate uptake of ce-MoS_2 nanosheets after 24 hours (Figures S7 and S8); there was no apparent degradation after 48 or 72 hours.

Author Manuscript Author Manuscript Author Manuscript Author Manuscript

Our findings have important implications for environmental health and safety. Chemically exfoliated MoS_2 nanosheets undergo a steady oxidative dissolution process in aqueous media over time scales of days to weeks, and are predicted to be non-persistent in living systems and the natural environment. Under the same conditions, bulk MoS_2 powders show no measurable dissolution over experimental time frames, highlighting that dissolution is a characteristic behavior of the ultrathin nanosheet form. The oxidative dissolution kinetics depend on media composition, and a pH-dependent kinetic law is developed for use in biokinetic or environmental fate modelling. Ultrasonically exfoliated MoS_2 nanosheets, show much slower oxidative dissolution rates, and the difference correlates with crystal phase, which varies from pure 2H in ue-MoS_2 to a 1T-rich composition in ce-MoS_2. These results are relevant for understanding the role of nanosheet/ion partitioning in the biological response of murine macrophages and human lung epithelial cells. Multiple entry pathways have been described for engineered nanoparticles that vary depending on their size, geometry, and chemical composition, as well as the target cell.[68] Depending on the uptake pathway, irregularly-shaped nanoparticles may escape from endosomes and avoid lysosomal compartmentalization and degradation or they may be sorted to lysosomes and rapidly degrade at low pH. A future comprehensive study of uptake mechanisms, compartmentalization, and intracellular degradation in a variety of potential target cells would be important for understanding potential adverse systemic responses following exposure to MoS_2 nanosheets.

Supplementary Material

Refer to Web version on PubMed Central for supplementary material.

Acknowledgments

Financial support for this work was provided by the Superfund Research Program of the National Institute of Environmental Health Sciences (Superfund Research Grant 2P42 ES013660), and the National Science Foundation (Grant INSPIRE Track 1 CBET-1344097).

References

1. Liu J, Wang Z, Liu FD, Kane AB, Hurt RH. Chemical Transformations of Nanosilver in Biological Environments. ACS Nano. 2012; 6:9887–9899. [PubMed: 23046098]
2. Xia T, Kovochich M, Liong M, Mädler L, Gilbert B, Shi H, Yeh JI, Zink JI, Nel AE. Comparison of the Mechanism of Toxicity of Zinc Oxide and Cerium Oxide Nanoparticles Based on Dissolution and Oxidative Stress Properties. ACS Nano. 2008; 2:2121–2134. [PubMed: 19206459]
3. Nel AE, Mädler L, Velegol D, Xia T, Hoek EM, Somasundaran P, Klaessig F, Castranova V, Thompson M. Understanding Biophysicochemical Interactions at the Nano–Bio Interface. Nat. Mater. 2009; 8:543–557. [PubMed: 19525947]
4. Kittler S, Greulich C, Diendorf J, Koller M, Epple M. Toxicity of Silver Nanoparticles Increases During Storage Because of Slow Dissolution under Release of Silver Ions. Chem. Mater. 2010; 22:4548–4554.
5. Wang Z, Von Dem Bussche A, Kabadi PK, Kane AB, Hurt RH. Biological and Environmental Transformations of Copper-Based Nanomaterials. ACS Nano. 2013; 7:8715–8727. [PubMed: 24032665]
6. Pietruska JR, Liu X, Smith A, McNeil K, Weston P, Zhitkovich A, Hurt R, Kane AB. Bioavailability, Intracellular Mobilization of Nickel, and HIF-1α Activation in Human Lung

Author Manuscript Author Manuscript Author Manuscript Author Manuscript

Epithelial Cells Exposed to Metallic Nickel and Nickel Oxide Nanoparticles. Toxicol. Sci. 2011; 124:138–148. [PubMed: 21828359]

7. Wang Z, Zhu W, Qiu Y, Yi X, von dem Bussche A, Kane A, Gao H, Koski K, Hurt R. Biological and Environmental Interactions of Emerging Two-Dimensional nanomaterials. Chem. Soc. Rev. 2016; 45:1750–1780. [PubMed: 26923057]
8. Stebounova LV, Guio E, Grassian VH. Silver Nanoparticles in Simulated Biological Media: a Study of Aggregation, Sedimentation, and Dissolution. J. Nanopart. Res. 2011; 13:233–244.
9. Setyawati MI, Yuan X, Xie J, Leong DT. The Influence of Lysosomal Stability of Silver Nanomaterials on their Toxicity to Human Cells. Biomaterials. 2014; 35:6707–6715. [PubMed: 24881025]
10. Peretyazhko TS, Zhang Q, Colvin VL. Size-Controlled Dissolution of Silver Nanoparticles at Neutral and Acidic pH Conditions: Kinetics and Size Changes. Environ. Sci. Techol. 2014; 48:11954–11961.
11. Kent RD, Vikesland PJ. Controlled Evaluation of Silver Nanoparticle Dissolution Using Atomic Force Microscopy. Environ. Sci. Techol. 2012; 46:6977–6984.
12. Bian S-W, Mudunkotuwa IA, Rupasinghe T, Grassian VH. Aggregation and Dissolution of 4 nm ZnO Nanoparticles in Aqueous Environments: Influence of pH, Ionic Strength, Size, and Adsorption of Humic Acid. Langmuir. 2011; 27:6059–6068. [PubMed: 21500814]
13. Setyawati MI, Tay CY, Leong DT. Mechanistic Investigation of the Biological Effects of SiO_2, TiO_2, and ZnO Nanoparticles on Intestinal Cells. Small. 2015; 11:3458–3468. [PubMed: 25902938]
14. Kent RD, Vikesland PJ. Dissolution and Persistence of Copper-Based Nanomaterials in Undersaturated Solutions with Respect to Cupric Solid Phases. Environ. Sci. Techol. 2015
15. Xiu, Z-m; Zhang, Q-b; Puppala, HL.; Colvin, VL.; Alvarez, PJ. Negligible Particle-Specific Antibacterial Activity of Silver Nanoparticles. Nano Lett. 2012; 12:4271–4275. [PubMed: 22765771]
16. Chen Y, Tan C, Zhang H, Wang L. Two-Dimensional Graphene Analogues for Biomedical Applications. Chem. Soc. Rev. 2015; 44:2681–2701. [PubMed: 25519856]
17. Huang J-K, Pu J, Hsu C-L, Chiu M-H, Juang Z-Y, Chang Y-H, Chang W-H, Iwasa Y, Takenobu T, Li L-J. Large-Area Synthesis of Highly Crystalline WSe_2 Monolayers and Device Applications. ACS Nano. 2014; 8:923–930. [PubMed: 24328329]
18. Smith RJ, King PJ, Lotya M, Wirtz C, Khan U, De S, O'Neill A, Duesberg GS, Grunlan JC, Moriarty G. Large-Scale Exfoliation of Inorganic Layered Compounds in Aqueous Surfactant Solutions. Adv. Mater. 2011; 23:3944–3948. [PubMed: 21796689]
19. Eda G, Yamaguchi H, Voiry D, Fujita T, Chen M, Chhowalla M. Photoluminescence from chemically exfoliated MoS_2. Nano Lett. 2011; 11:5111–5116. [PubMed: 22035145]
20. Lukowski MA, Daniel AS, English CR, Meng F, Forticaux A, Hamers RJ, Jin S. Highly Active Hydrogen Evolution Catalysis from Metallic WS_2 Nanosheets. Energy & Environmental Science. 2014; 7:2608–2613.
21. Zhang H. Ultrathin Two-Dimensional Nanomaterials. ACS Nano. 2015; 9:9451–9469. [PubMed: 26407037]
22. Li H, Wu J, Yin Z, Zhang H. Preparation and Applications of Mechanically Exfoliated Single-Layer and Multilayer MoS_2 and WSe_2 Nanosheets. Acc. Chem. Res. 2014; 47:1067–1075. [PubMed: 24697842]
23. Huang X, Tan C, Yin Z, Zhang H. 25th Anniversary Article: Hybrid Nanostructures Based on Two - Dimensional Nanomaterials. Adv. Mater. 2014; 26:2185–2204. [PubMed: 24615947]
24. Tan C, Zhang H. Two-Dimensional Transition Metal Dichalcogenide Nanosheet-Based Composites. Chem. Soc. Rev. 2015; 44:2713–2731. [PubMed: 25292209]
25. Zeng Z, Yin Z, Huang X, Li H, He Q, Lu G, Boey F, Zhang H. Single - Layer Semiconducting Nanosheets: High - Yield Preparation and Device Fabrication. Angew. Chem. Int. Ed. 2011; 50:11093–11097.
26. Mak KF, Lee C, Hone J, Shan J, Heinz TF. Atomically Thin MoS_2: a New Direct-Gap Semiconductor. Phys. Rev. Lett. 2010; 105:136805. [PubMed: 21230799]

Author Manuscript Author Manuscript Author Manuscript Author Manuscript

27. Radisavljevic B, Radenovic A, Brivio J, Giacometti V, Kis A. Single-Layer MoS_2 Transistors. Nat. Nanotechnol. 2011; 6:147–150. [PubMed: 21278752]
28. Mouri S, Miyauchi Y, Matsuda K. Tunable Photoluminescence of Monolayer MoS_2 via Chemical Doping. Nano Lett. 2013; 13:5944–5948. [PubMed: 24215567]
29. Yin Z, Li H, Li H, Jiang L, Shi Y, Sun Y, Lu G, Zhang Q, Chen X, Zhang H. Single-Layer MoS_2 Phototransistors. ACS Nano. 2011; 6:74–80. [PubMed: 22165908]
30. Li H, Yin Z, He Q, Li H, Huang X, Lu G, Fam DWH, Tok AIY, Zhang Q, Zhang H. Fabrication of Single - and Multilayer MoS_2 Film - Based Field - Effect Transistors for Sensing NO at Room Temperature. Small. 2012; 8:63–67. [PubMed: 22012880]
31. Chhowalla M, Shin HS, Eda G, Li L-J, Loh KP, Zhang H. The Chemistry of Two-Dimensional Layered Transition Metal Dichalcogenide Nanosheets. Nat. Chem. 2013; 5:263–275. [PubMed: 23511414]
32. Baysinger, G. CRC Handbook of Chemistry and Physics. National Institute of Standards and Technology; 2015.
33. Li Y, Zhou Z, Zhang S, Chen Z. MoS_2 Nanoribbons: High Stability and Unusual Electronic and Magnetic Properties. J. Am. Chem. Soc. 2008; 130:16739–16744. [PubMed: 19554733]
34. Santosh K, Longo RC, Wallace RM, Cho K. Surface Oxidation Energetics and Kinetics on MoS_2 Monolayer. J. Appl. Phys. 2015; 117:135301.
35. Ross S, Sussman A. Surface Oxidation of Molybdenum Disulfide. J. Phys. Chem. 1955; 59:889–892.
36. Yamamoto M, Einstein TL, Fuhrer MS, Cullen WG. Anisotropic Etching of Atomically Thin MoS_2. J. Phys. Chem. 2013; 117:25643–25649.
37. Liu Y, Tan C, Chou H, Nayak A, Wu D, Ghosh R, Chang H-Y, Hao Y, Wang X, Kim J-S. Thermal Oxidation of WSe_2 Nanosheets Adhered on S_iO_2/Si Substrates. Nano Lett. 2015; 15:4979–4984. [PubMed: 26171759]
38. Gao J, Li B, Tan J, Chow P, Lu T-M, Koratkar N. Aging of Transition Metal Dichalcogenide Monolayers. ACS Nano. 2016; 10:2628–2635. [PubMed: 26808328]
39. Mancini MC, Kairdolf BA, Smith AM, Nie S. Oxidative Quenching and Degradation of Polymer-Encapsulated Quantum Dots: New Insights into the Long-Term Fate and Toxicity of Nanocrystals *in vivo*. J. Am. Chem. Soc. 2008; 130:10836–10837. [PubMed: 18652463]
40. Pichaandi J, Abel KA, Johnson NJ, van Veggel FC. Long-Term Colloidal Stability and Photoluminescence Retention of Lead-Based Quantum Dots in Saline Buffers and Biological Media through Surface Modification. Chem. Mater. 2013; 25:2035–2044.
41. Li BL, Chen LX, Zou HL, Lei JL, Luo HQ, Li NB. Electrochemically Induced Fenton Reaction of Few-Layer MoS_2 Nanosheets: Preparation of Luminescent Quantum Dots via a Transition of Nanoporous Morphology. Nanoscale. 2014; 6:9831–9838. [PubMed: 25027566]
42. Guardia L, Paredes JI, Munuera JM, Villar-Rodil S, Ayán-Varela M, Martínez-Alonso A, Tascón JM. Chemically Exfoliated MoS_2 Nanosheets as an Efficient Catalyst for Reduction Reactions in the Aqueous Phase. ACS Appl. Mater. Interfaces. 2014; 6:21702–21710. [PubMed: 25405770]
43. Liu J, Hurt RH. Ion Release Kinetics and Particle Persistence in Aqueous Nano-Silver Colloids. Environ. Sci. Techol. 2010; 44:2169–2175.
44. Wypych F, Schollhorn R. 1T-MoS_2, a New Metallic Modification of Molybdenum Disulfide. J. Chem. Soc., Chem. Commun. 1992:1386–1388.
45. Chou SS, De M, Kim J, Byun S, Dykstra C, Yu J, Huang J, Dravid VP. Ligand Conjugation of Chemically Exfoliated MoS_2. J. Am. Chem. Soc. 2013; 135:4584–4587. [PubMed: 23472859]
46. Py M, Haering R. Structural Destabilization Induced by Lithium Intercalation in MoS_2 and Related Compounds. Can. J. Phys. 1983; 61:76–84.
47. Bertolazzi S, Brivio J, Kis A. Stretching and Breaking of Ultrathin MoS_2. ACS Nano. 2011; 5:9703–9709. [PubMed: 22087740]
48. Lembke D, Kis A. Breakdown of High-Performance Monolayer MoS_2 Transistors. ACS Nano. 2012; 6:10070–10075. [PubMed: 23039374]

Author Manuscript Author Manuscript Author Manuscript Author Manuscript

49. Chou SS, Kaehr B, Kim J, Foley BM, De M, Hopkins PE, Huang J, Brinker CJ, Dravid VP. Chemically Exfoliated MoS_2 as Near-Infrared Photothermal Agents. Angew. Chem. Int. Ed. 2013; 52:4160–4164.
50. Liu T, Wang C, Gu X, Gong H, Cheng L, Shi X, Feng L, Sun B, Liu Z. Drug Delivery with PEGylated MoS_2 Nano-Sheets for Combined Photothermal and Chemotherapy of Cancer. Adv. Mater. 2014; 26:3433–3440. [PubMed: 24677423]
51. Ju H, Jia L, Ding L, Tian J, Bao L, Hu Y, Yu J-S. Aptamer Loaded MoS_2 Nanoplates as Nanoprobe for Detection of Intracellular ATP and Controllable Photodynamic Therapy. Nanoscale. 2015; 7:15953–15961. [PubMed: 26367253]
52. Chow PK, Singh E, Viana BC, Gao J, Luo J, Li J, Lin Z, Elías AL, Shi Y, Wang Z. Wetting of Mono and Few-Layered WS_2 and MoS_2 Films Supported on Si/SiO_2 Substrates. ACS Nano. 2015; 9:3023–3031. [PubMed: 25752871]
53. Chow PK, Jacobs-Gedrim RB, Gao J, Lu T-M, Yu B, Terrones H, Koratkar N. Defect-Induced Photoluminescence in Monolayer Semiconducting Transition Metal Dichalcogenides. ACS Nano. 2015; 9:1520–1527. [PubMed: 25603228]
54. Ding Q, Meng F, English CR, Cabán-Acevedo M, Shearer MJ, Liang D, Daniel AS, Hamers RJ, Jin S. Efficient Photoelectrochemical Hydrogen Generation Using Heterostructures of Si and Chemically Exfoliated Metallic MoS_2. J. Am. Chem. Soc. 2014; 136:8504–8507. [PubMed: 24892384]
55. Chng ELK, Sofer Z, Pumera M. MoS_2 Exhibits Stronger Toxicity with Increased Exfoliation. Nanoscale. 2014; 6:14412–14418. [PubMed: 25341082]
56. Teo WZ, Chng ELK, Sofer Z, Pumera M. Cytotoxicity of Exfoliated Transition - Metal Dichalcogenides (MoS_2, WS_2, and WSe_2) is Lower Than That of Graphene and its Analogues. Chem. Eur. J. 2014; 20:9627–9632. [PubMed: 24976159]
57. Fan J, Li Y, Nguyen HN, Yao Y, Rodrigues DF. Toxicity of Exfoliated-MoS_2 and Annealed Exfoliated-MoS_2 towards Planktonic Cells, Biofilms, and Mammalian Cells in the Presence of Electron Donor. Environ. Sci. Nano. 2015; 2:370–379.
58. Shah P, Narayanan TN, Li C-Z, Alwarappan S. Probing the Biocompatibility of MoS_2 Nanosheets by Cytotoxicity Assay and Electrical Impedance Spectroscopy. Nanotechnology. 2015; 26:315102. [PubMed: 26183754]
59. Chen S, Wang L-W. Thermodynamic Oxidation and Reduction Potentials of Photocatalytic Semiconductors in Aqueous Solution. Chem. Mater. 2012; 24:3659–3666.
60. Liu W, Yang X, Zhang Y, Xu M, Chen H. Ultra-Stable Two-Dimensional MoS_2 Solution for Highly Efficient Organic Solar Cells. RSC Adv. 2014; 4:32744–32748.
61. Heising J, Kanatzidis MG. Exfoliated and Restacked MoS_2 and WS_2: Ionic or Neutral Species? Encapsulation and Ordering of Hard Electropositive Cations. J. Am. Chem. Soc. 1999; 121:11720–11732.
62. Tay CY, Setyawati MI, Xie J, Parak WJ, Leong DT. Back to Basics: Exploiting the Innate Physico - chemical Characteristics of Nanomaterials for Biomedical Applications. Adv. Funct. Mater. 2014; 24:5936–5955.
63. Eda G, Fujita T, Yamaguchi H, Voiry D, Chen M, Chhowalla M. Coherent Atomic and Electronic Heterostructures of Single-Layer MoS_2. ACS Nano. 2012; 6:7311–7317. [PubMed: 22799455]
64. Bosecker K. Bioleaching: Metal Solubilization by Microorganisms. FEMS Microbiol. Rev. 1997; 20:591–604.
65. Schippers A, Sand W. Bacterial Leaching of Metal Sulfides Proceeds by Two Indirect Mechanisms via Thiosulfate or via Polysulfides and Sulfur. Appl. Environ. Microbiol. 1999; 65:319–321. [PubMed: 9872800]
66. Bryner L, Anderson R. Microorganisms in Leaching Sulfide Minerals. Ind. Eng. Chem. 1957; 49:1721–1724.
67. Zhang XD, Chen J, Min Y, Park GB, Shen X, Song SS, Sun YM, Wang H, Long W, Xie J. Metabolizable Bi_2Se_3 Nanoplates: Biodistribution, Toxicity, and Uses for Cancer Radiation Therapy and Imaging. Adv. Funct. Mater. 2014; 24:1718–1729.
68. Lee DS, Qian H, Tay CY, Leong DT. Cellular Processing and Destinies of Artificial DNA Nanostructures. Chem. Soc. Rev. 2016

Author Manuscript Author Manuscript Author Manuscript Author Manuscript

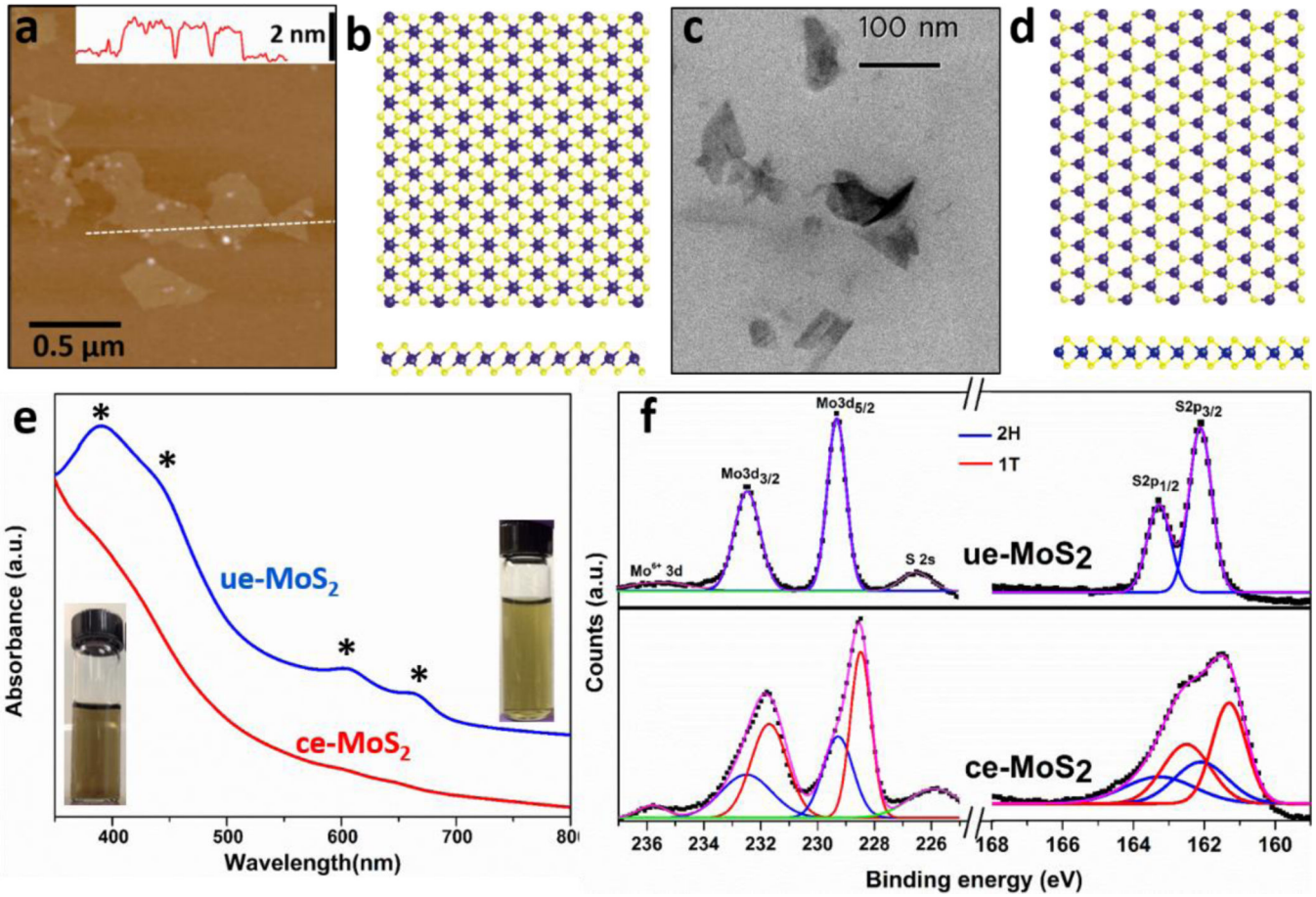

Figure 1.

Structure and crystal phases of MoS_2 nanosheets fabricated for this study. (**a**) AFM image of ce-MoS_2 nanosheets, inset: line scan showing the thickness profile along the dash line in the AFM image; (**b**) atomic positions in the 1T phase with octahedral coordination, (**c**) STEM image of ue-MoS_2 nanosheets, (**d**) atomic positions in the 2H phase with trigonal prismatic coordination. (**e**) UV-vis absorbance of ue-MoS_2 (blue trace) and ce-MoS_2 (red trace) with the characteristic peaks of the 2H phase marked by asterisks. Inset: digital photographs of as-prepared ce-MoS_2 (left) and ue-MoS_2 (right) dispersions showing uniformity. (**f**) XPS spectra and deconvolution analysis (Mo 3d and S 2p) showing that ue-MoS_2 is in the 2H phase, and ce-MoS_2 has mixed 1T and 2H phases.

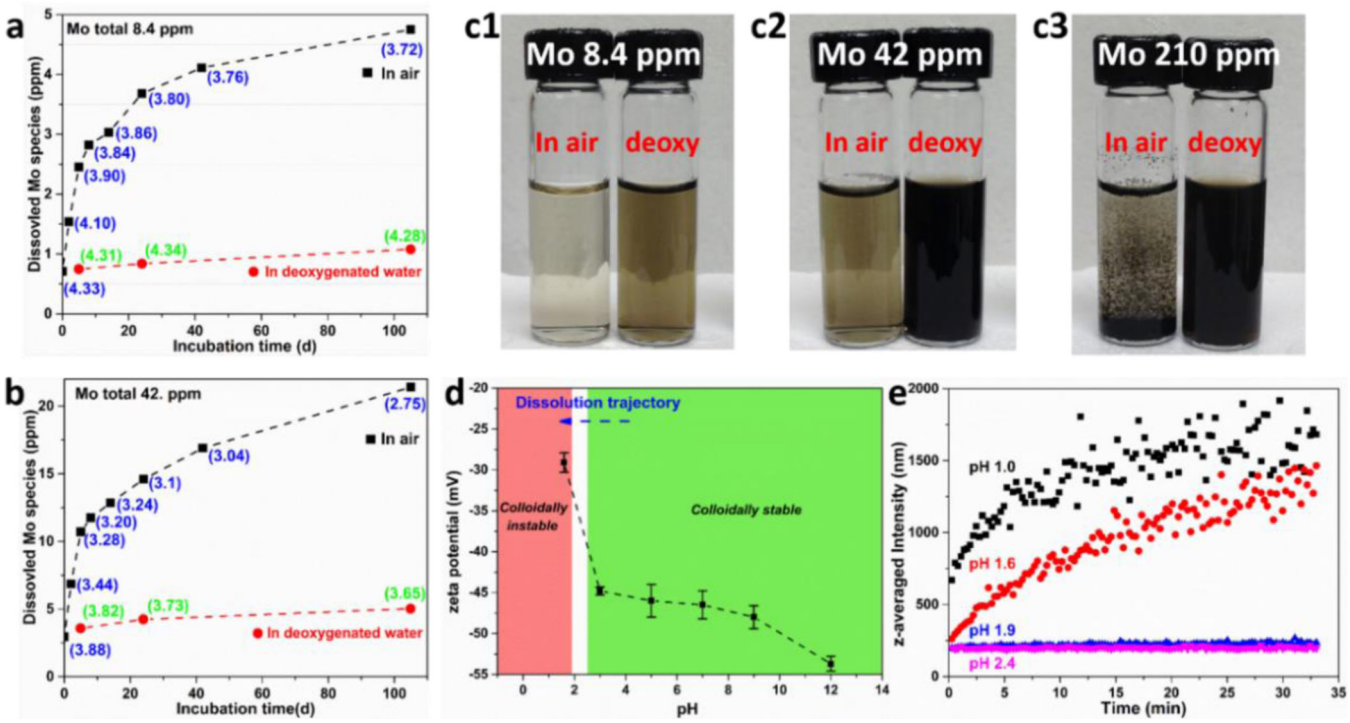

Figure 2.

Oxidative dissolution and colloidal stability of ce-MoS_2. Dissolution of ce-MoS_2 nanosheets at low (**a**) and intermediate starting concentration (**b**) in air-saturated water, but does not occur in deoxygenated water (**a,b**). This oxidative dissolution process produces protons (pH values given in parentheses), and the pH evolution in (**a**) and (**b**) are consistent with the hypothesized oxidation reaction in Eq. 1. (**c**) Photographs showing that ce-MoS_2 is colloidally stable in all dispersions after 105-day incubation except at the highest starting Mo concentrations (210 ppm) in O_2-containing water, which produces the highest proton concentrations. This suggests that aggregation of these negatively charged nanosheets is induced by low pH, which is confirmed by the measurements of zeta potentials (**d**) and hydrodynamic sizes (**e**) at various pH values. Dynamic light scattering was used to measure the change, and the pH of the solution was adjusted by addition of HCl or NaOH to ce-MoS_2 solution (~10 ppm of Mo). Higher resolution view of DLS measurement at pH~2 region can be found in the Supporting Information, Fig. S4.

Author Manuscript Author Manuscript Author Manuscript Author Manuscript

Author Manuscript Author Manuscript Author Manuscript Author Manuscript

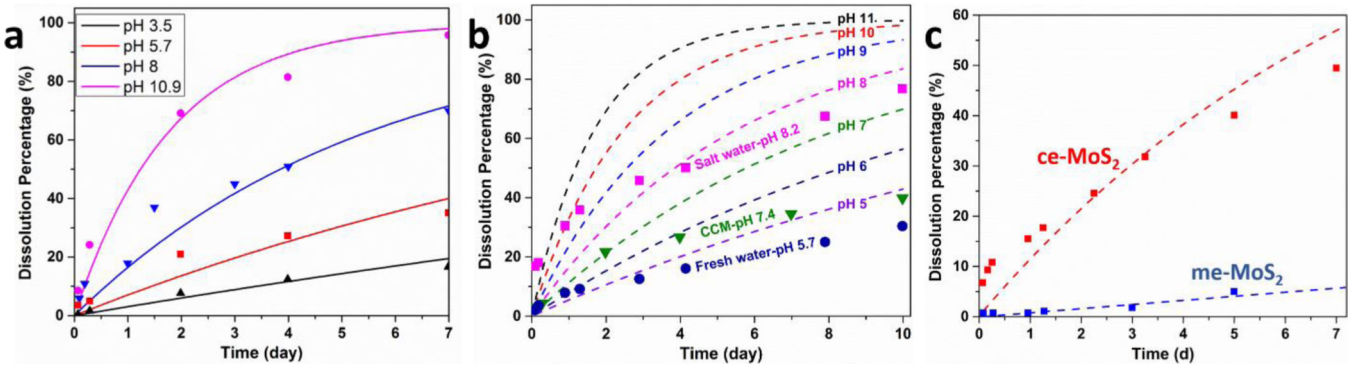

Figure 3.

Kinetics of pH-dependent oxidative dissolution and complex media effects. (**a**) pH-dependent dissolution rates obtained using various buffer solutions. The lines show results of an empirical kinetic law (Eq. 2) fit to this data set. (**b**) Dissolution in complex media (data points) compared to simple media (dash lines, representing model in (**a**)). (**c**) Dissolution rates for chemically vs. ultrasonically exfoliated MoS_2 nanosheets in HEPES buffers (pH 7). Both undergo continuous dissolution, but the kinetics are much slower for the ue-MoS_2 samples.

Author Manuscript Author Manuscript Author Manuscript Author Manuscript

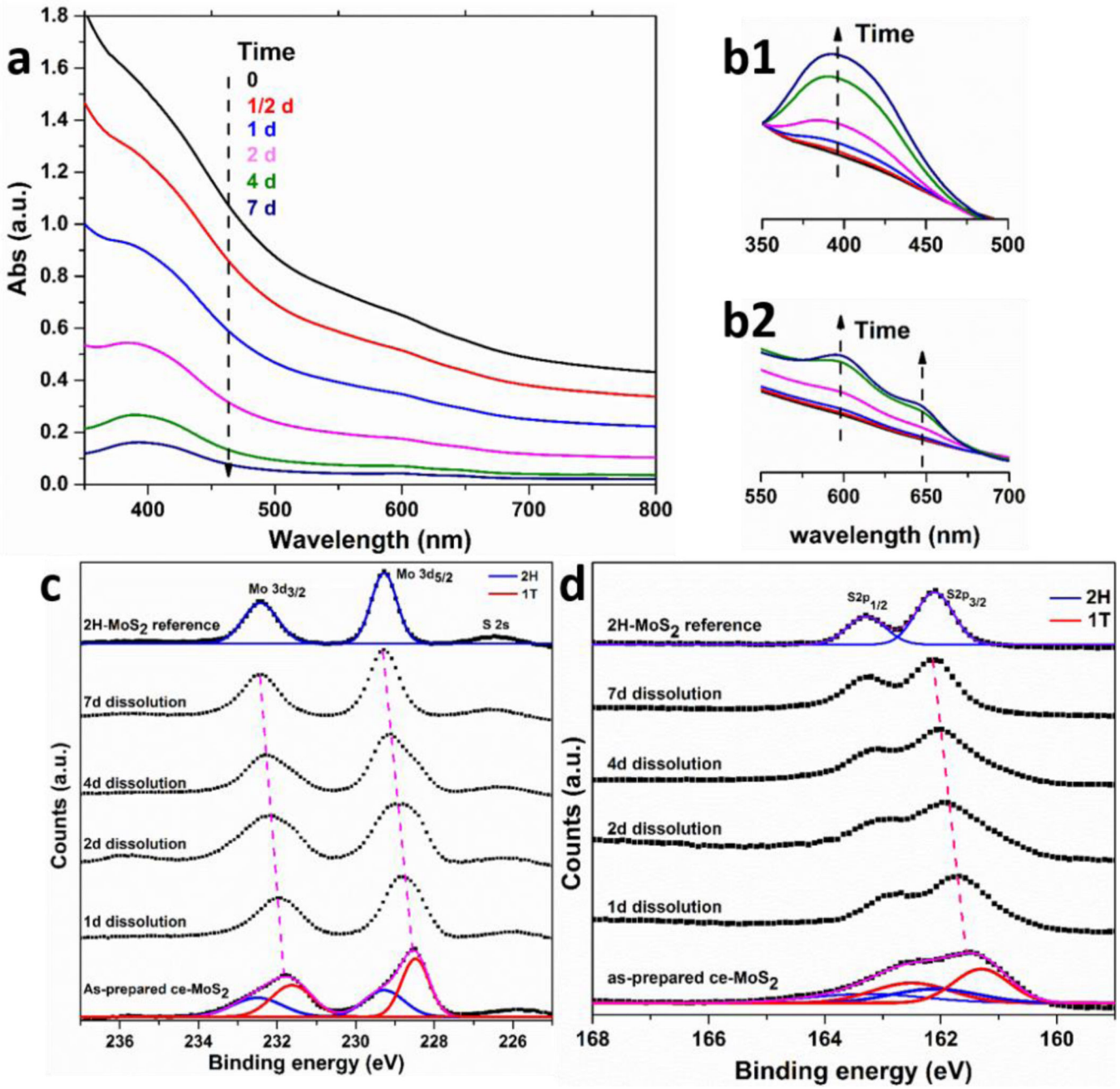

Figure 4.

Preferential oxidation of 1T phase over 2H phase. (**a**) The evolution of UV-vis spectra as a result of oxidative dissolution of ce-MoS_2 in high pH buffer (pH ~11.2). The increase of normalized peak intensities at ~ 400 nm (**b1**, normalized at 350 nm) and ~ 600 to 650 nm (**b2**, normalized at 800 nm) indicates the preferential oxidation of 1T phase and enrichment of 2H phase. XPS spectra showing Mo 3d (**c**) and S 2p (**d**) peak regions for samples treated for different periods of time. The overall convolution peaks are observed to shift to higher binding energies implying the fast decomposition of 1T phase with lower binding energies. 2H phase becomes the only component after 7-day dissolution.

Author Manuscript Author Manuscript Author Manuscript Author Manuscript

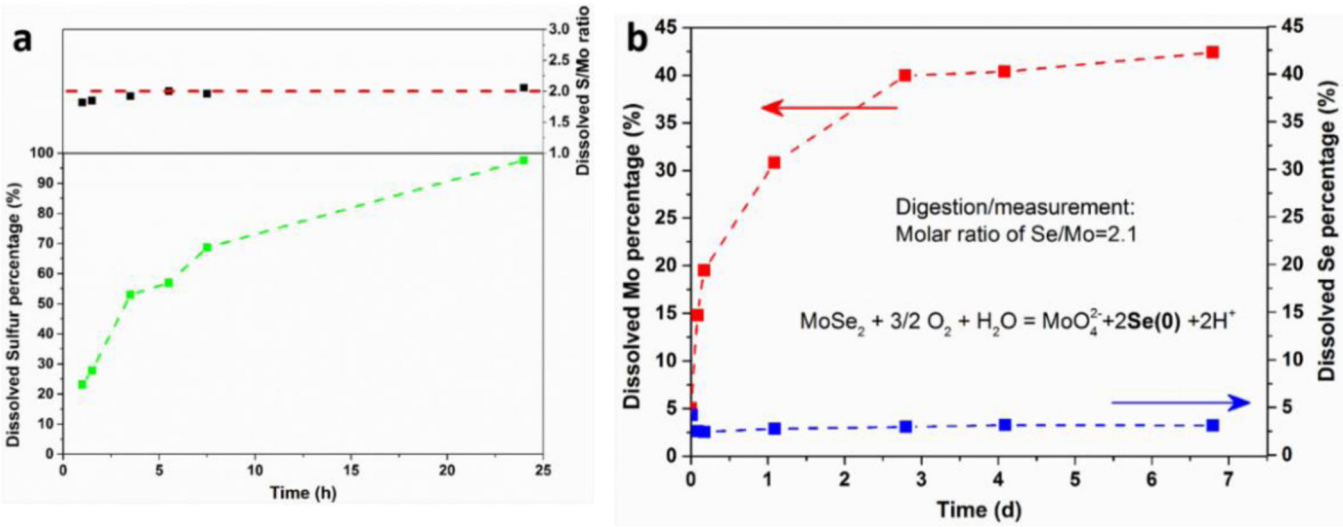

Figure 5.

Analysis of secondary reaction products in the oxidative dissolution of MoS_2 and $MoSe_2$. (**a**) Time-resolved appearance of soluble sulfur species when ce-MoS_2 sample is incubated in pH 12 solution. The ratio of S/Mo in the filtrate is close to 2, suggesting uniform degradation of MoS_2 and release of all soluble products. (**b**) As a comparison, ce-$MoSe_2$ can also undergo oxidative dissolution (pH 7.4) releasing soluble Mo, but the chalcogen product is presumably insoluble Se(0).

Author Manuscript Author Manuscript Author Manuscript Author Manuscript

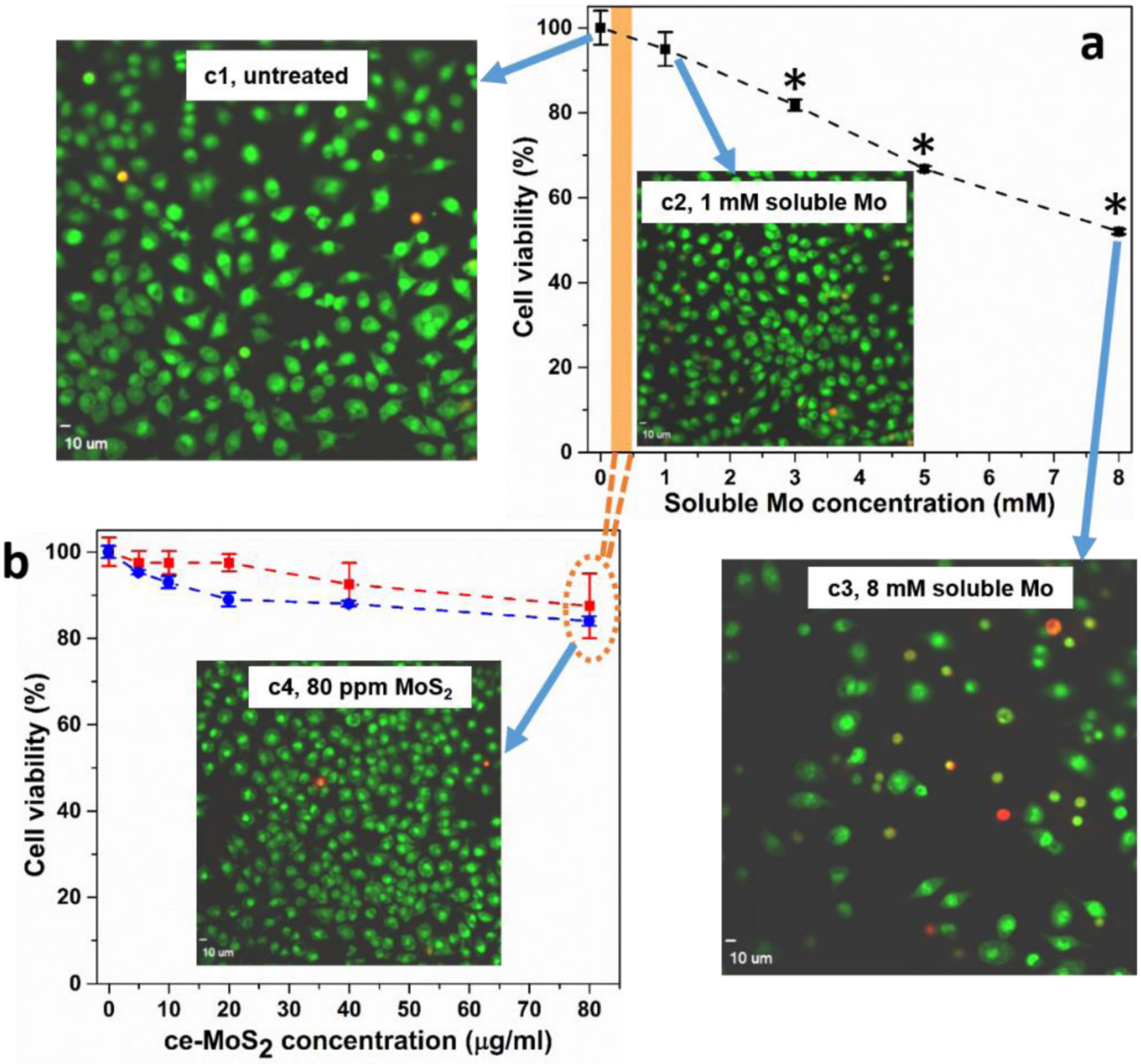

Figure 6.

Cytotoxicity for murine macrophages of ce-MoS_2 nanosheets and soluble molybdate ions. Assessment of cell viability after exposure of murine macrophages to different concentrations of Mo salt (**a**) and ce-MoS_2 sample (**b**). Following exposure to various amounts of Mo salt for 1 d or ce-MoS_2 samples for 1 (red trace) or 2 days (blue trace), viability was assessed using dehydrogenase activity assay Wst 8. Concentrations above 3 mM Mo salt caused a significant decrease of viability (*$p < 0.05$). There was no significant cell death measured within 2 days of treatment in nanosheet samples. Images show visualization of cell death in murine macrophages using ethidium homodimer/Syto 10 stain after exposure to Mo salt or ce-MoS_2 nanosheets for 24 hours. Macrophages were seeded into 96 well plates and imaged using an Olympus confocal microscope to visualize live

Author Manuscript Author Manuscript Author Manuscript Author Manuscript

(green) and dead (red) cells. Cells exposed to 8 mM Mo salt (**c3**) show significant loss in cell count and strong red fluorescence, while unexposed cells (**c1**), cells exposed to 1 mM Mo salt (**c2**), 80 μg/ml MoS_2 nanosheets (**c4**) do not show toxicity, shown by strong green fluorescence. Images demonstrating uptake of ce-MoS_2 by murine macrophages and human lung epithelial cells can be found in Supporting Information, Fig. S8